Toward a method of understanding the complexation of rare earth element by functionalized organosilanes in aqueous media

Oliver Walker, Diane Rébiscoul, Michael Odorico, Samuel Tardif, Stephane Pellet-Rostaing, Guilhem Arrachart

GRAPHICAL ABSTRACT

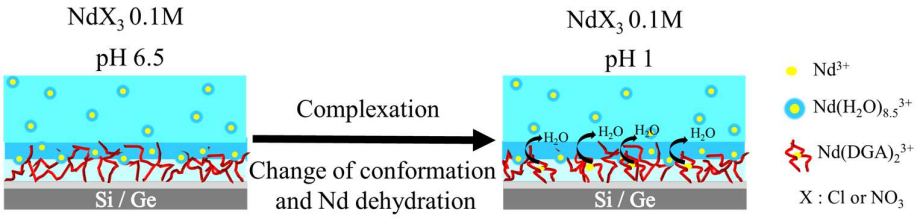

Toward a method of understanding the complexation of Rare Earth Element by functionalized organosilanes in aqueous media

Oliver Walker†‡, Diane Rébiscoul *†, Michael Odorico† , Samuel Tardif #, Stephane Pellet-Rostaing†, Guilhem Arrachart†

† Univ Montpellier, ICSM, CNRS, CEA, ENSCM, Bagnols Sur Cèze, France

olivier.walker@cea.fr; diane.rebiscoul@cea.fr; michael.ordorico@cea.fr; stephane.pellet-rostaing@cea.fr; Guilhem.arrachart@cea.fr

CEA, IRIG-MEM Univ. Greonble Alpes F-38000 Grenoble, France

Samuel.tardif@cea.fr

‡ Present address Institute of Physical Chemistry, University of Stuttgart, 70569 Stuttgart, Germany

Corresponding author: diane.rebiscoul@cea.fr ; tel: 0033 4 66 33 93 30

ABSTRACT

In the context or rare earth element extraction using solid-liquid process, hybrid materials having specific functional group were largely studied. However, there is a lack of *in situ* characterization method to understand how the functional group behaves when interacts with the rare earth element. Here, we propose a new experimental method to understand the interaction between immobilized functional group and REE in aqueous media using a well-characterized model system coupled to surface analyses. Model system was prepared by grafting diglycolamide functionalized silane on planar silica substrate. In order

to have a clear description of the morphology and the structure of the model system, the silane grafting process was characterized using contact angle measurement, X-Ray Reflectivity, peak force measurements by Atomic Force Microscopy and in situ analysis by Fourier Transformed Infrared Spectroscopy in Attenuated Total Reflection. Afterwards, the behavior of the grafted molecules was investigated in neodymium aqueous solution at various pH by *in situ* infrared spectroscopy and hard X-ray reflectivity characterizations. Here, we highlight that the complexation of Nd^{3+} by the diglycolamide function is correlated with its dehydration and a modification of the molecule configuration.

KEYWORDS : REE extraction; diglycolamide; Grafting; Complexation; I*n situ* Hard X-ray reflectivity, *In situ* infrared spectroscopy

INTRODUCTION

The critical raw materials access is becoming more and more difficult due to resource accessibility and a complex geopolitics context [1-2]. Their recycling from industrial wastes such as production scraps and end-of-life products also called “Urban mine”, admittedly complex, appears as an opportunity to ensure the independence and the competitiveness of the country economy and to propose a global effective circular economy. This approach decreases the need for primary resources and prevents end-of-life products from being landfilled.

Today, technologies used to recover critical raw materials such as Rare Earth Elements (REEs) used in various technologies and particularly in electronic and energy sector, are based on various processes such as mechanical recycling, hydro-metallurgical, pyro-metallurgical, electro-metallurgical, bio-metallurgical processes, and their combinations [3-6]. Liquid-liquid extraction processes are still optimized by experimental plan varying parameters because the ienaics colloidal approach, also known as Gibbs-Energy Miminization method [7], is not developed sufficiently to go beyond the rationalization of the experimental results [8-9]. Indeed, the extraction of elements from complex fluids [10] having thermodynamic properties that are still under investigation are very sensitive to the variability of the waste

leachate composition that can strongly modify the extraction process efficiency. In contrast, solid-liquid extraction is more robust and considered as one of the most promising REE extraction and recovery options. This kind of extraction is easy to implement, low cost, available, avoids the use of organic solvent during the process [11] and generally presents high removal efficiencies even with effluent presenting low element concentrations. In addition, the elements can be recovered simply by a change of pH [12-13] and it has been demonstrated that some solid sorbents can be reused several times with good extractive capacity [14-19].

Hybrid materials were largely studied for REE extraction. These materials are generally prepared by polycondensation or by grafting on various substrates (nanoparticle or pore surfaces to maximize the reactive surface) of functionalized organosilanes [15,16,20-28], having selective headgroups regarding REEs. These selective headgroups are essential since competitive ions can be present in leachates. Generally, these functions are able either to exchange proton with REEs either to chelate REEs such as carboxylic acid group, phosphorus, tertiary amine coupled with either carboxylic or ester moieties, amide-based groups [14, 15, 29-32]. One of the most interesting function is the diglycolamide-type. This function is neutral in a large pH range, has a strong selectivity regarding REEs forming 1:3 complex and present a lower affinity over competing elements such Al, Fe, Th, and U [33-36]. Several organosilanes with diglycolamide function have been already used to graft mesopores of silica such as SBA-15 or KIT-6 [16, 18,23,32] and for the fabrication of silica-hybrid materials using 1-pot synthesis [21,37,38]. These materials have presented a high extraction efficiency and selectivity regarding REEs which depend on pH [21,39,40]. The affinity of REEs to be chelated by the three oxygen atoms of the diglycolamide function depends on the so-called “bite-angle”, *i.e*. the angle between the three oxygen atoms in the function. This angle can be modified by the nature of the diglycolamine molecule and its tethering within the material that pilot its ability to warp [16,18,23,36], and thus affect its affinity for REEs. Currently, all of these results comes from extraction studies and not *in situ* characterization of the hybrid materials when it contacts aqueous solution containing REEs.

In situ Fourier Transformed Infrared Spectroscopy in Attenuated Total Reflection (FTIR-ATR) is an interesting tool to study solid-liquid interface [40] and particularly to determine how molecules directly deposited on the crystal used to probe the surface, behave when they contact a liquid. Combined with *in situ* neutron reflectometry, these two techniques give complementary information about the evolutions of the structure of the molecules in contact with the liquid and their organization perpendicular to the surface [41,42]. Generally, this tool combination, FTIR-ATR and reflectometry, was applied to lipids, surfactants and polymers directly adsorbed on the crystal surface but never on molecules such as organosilanes, directly grafted on the crystal. Because several reactions can compete with the condensation of the molecules with the hydroxyls of substrate surface as the self-condensation and the physisorption [43], it is essential to have a perfect knowledge of the structure and the morphology of the grafted layer to correctly interpret the molecule behavior in aqueous solution.

Regarding this context, we propose for the first time, an experimental method to better understand how functionalized organosilanes behave in contact with REE in aqueous media using a well-characterized model system coupled to *in situ* surface analyses such as FTIR-ATR and hard X-ray reflectivity. For this purpose, we prepared a model system based on the grafting of diglycolamide functionalized silane (DGA) on planar substrate. Based on our previous works [43,44] and in order to have a clear description of the morphology and the structure of the model system, the DGA grafting process was characterized using contact angle measurement, X-Ray Reflectivity (XRR), peak force measurements by Atomic Force Microscopy (AFM) and *in situ* analysis by FTIR-ATR. Afterwards, we investigated the behavior of the grafted molecules in $NdCl_3$ aqueous solution at 0.1 M at various pH by *in situ* FTIR-ATR as in [45,40] and hard X-ray reflectivity characterizations. Here, we highlight that the complexation of Nd^{3+} by DGA goes with its dehydration and a modification of the DGA configuration. Even if this model system does not represent the complexity of a real hybrid materials surface (surface curvature, conformation of organosilanes, orientation and geometry of the functional group) in contact with REE aqueous solution,

it helps to understand the functional group behavior and give access to new results that was not *in situ* characterized until now.

MATERIALS AND METHODS

Organosilane synthesis

The synthesis of the organosilane precursor is based on the use of click chemistry starting from 11-azidoundecyl triethoxysilane as described in the work of Besnard et al. [37], and propargyl-dioctyldiglycolamide (DODGA) by applying the procedure introduced by Wehbie et al. [46]. The subsequent click chemistry between the Azido triethoxysilane precursor and the propargyl-DODGA was performed by the optimized procedure described by Winkler et al. [38]. Therefore, under N_2 atmosphere, [Cu(C18tren)Br] catalyst (Sigma Aldrich, 99.99%) (0.04 mmol, 0.01 eq.) was dissolved in 24 mL of toluene (Carlo Erba, 99%). The azido triethoxysilane precursor (4 mmol, 1 eq.) and propargyl-DODGA (6 mmol, 1.5 eq.), were added. The obtained solution was stirred for 5 h at 40°C. The solvent was then evaporated at 10 mbar and 50 °C. The residue was dissolved in 20 mL of anhydrous ethanol (Acros organics, 99.5%) and stored at -4 °C overnight. The solution was filtrated by using 0.2 µm syringe filters. The residual ethanol was again evaporated affording in a viscous green-brown oil consisting of the DGA triethoxysilane(2-(2-oxo-2-(((1-(11-(triethoxysilyl)undecyl)-1H-1,2,3-triazole-4-yl)methyl)amino)ethoxy)-N,N-dipropylacetamide). The success of the DGA triethoxysilane synthesis was confirmed by NMR- and ATR-FTIR- spectroscopy. The results are provided in Figure S1 and Figure S2 in supporting information.

Sample preparation

Silicon wafers (MEMC elect. Materials, P-type) of 1x1 cm² was activated to form surface hydroxyl groups under reflux in 10% HNO_3 (Carlo Erba, 69%) for 24 h at 160°C. Afterward, the wafers were rinsed three times with ultrapure water. Based on the grafting procedure of McGovern et al. [47], one side of the activated wafers was put in contact with a solution constituted of 1 wt. % organosilane diluted in toluene

(Carlo Erba, 99%) during 30 min, 1h and 19h. During the grafting process, a dried nitrogen flow was maintained above the solution to avoid water uptake from the laboratory atmosphere. This allows a limitation of the organosilane polycondensation. After this step, the samples were rinsed with toluene and dried under N_2. At the end of the process, the samples were stored under vacuum.

***Ex situ* characterization**

X-ray reflectivity (XRR) measurements were performed to determine the electron density profile of the samples using a Brüker D8 diffractometer with Cu Kα1 X-ray source (λ = 1.54056 nm). Data were collected from 0° to 3° with an angular resolution of 0.01°. After a rescaling of the illuminated surface area and a normalization by the direct beam I0, the reflectivity curves were presented as the evolution of the logarithm of intensity I/I0 as a function of the wave vector $q = \frac{4\pi \sin_i}{\lambda}$ with θ_i the incident angle. Layer thickness and electron density profiles were obtained by fitting the experimental data with the Firefx4c_6 software [48] based on the Parratt algorithm [49].

Water contact angles of the surface of the samples were measured at room temperature using a Kruss Drop Shape Analyzer DSA100. A 10 µL drop volume was deposited at the surface of the sample with a flow rate of 600 µL/min. The contact angle out of a sessile drop was calculated using the DSA1 v1.91 software with the Young–Laplace method. This operation was repeated three times. Data are presented as an average value of three measurements including the standard deviation.

The surface layer morphology, i.e. the roughness and the spatial organization of the grafted organosilanes were characterized by Atomic Force Microscopy (AFM) using a MultiMode8 with NanoScope V from Brüker. The peak force measurements were performed with the same tip (SNL 0.35 Nm 0from BRUCKER). All the measurements were performed at the same laboratory atmosphere to avoid artefacts of the water meniscus [50]. Cantilever calibration was performed by the thermal tune method with a hard “naked” silicon substrate and the spring constant was set to 280 pN nm^{-1}. For each sample, 30 forces curves including an approach and a retract curves were recorded. For approach curves,

analyzed parameters were the tip−surface attraction force and the distance for retract curves tip−surface adhesion force (F) and adhesion length (L) respectively. [51]

***In situ* characterization**

In situ ATR-FTIR measurements were performed by using a PerkinElmer Spectrum 100 FT-IR Spectrometer in ATR mode equipped with a DTGS/KBR detector and a Horizontal Attenuated Total Reflectance (HATR) Flow-Through Cell from PIKE Technologies. The ATR Ge crystal with a refractive index of $n = 4$ was used as a substrate to directly characterize in situ the grafting process as in published work [52]. Analysis were performed at 45°. Each scan was the average of 4 scans with a resolution of 4 cm^1. Before each measurement, the Ge crystal surface was activated to form surface Ge-OH groups as proposed in the literature [52,53] For this, the Ge crystal was separated from the measurements cell and placed in a 9:1 v/v mixture of H_2O_2 35 w% (Acros organics) and oxalic acid 99 w% (Sigma Aldrich) for 5 minutes subsequently rinsed with water and dried in a N_2 stream. Afterward, the crystal was placed in the measurement cell and the background was recorded. In a next step, the cell was flushed with toluene (Carlo Erba, 99%) and measurement was recorded. For the recording of the grafting kinetics of the organosilane, the toluene was replaced by a solution of 1 wt. % of organosilane dissolved in toluene. Spectra were recorded each 20 minutes until no evolution of the spectra was observed. At the end of the grafting process, the cell was rinses three times with toluene to remove unbounded organosilanes and finally dried with a N_2 flux. To investigate the interactions between the grafted organosilanes and the aqueous solution, the cell was first filled with ultrapure water and spectra were recorded until no evolution was observed. Second, aqueous solutions of $NdCl_3$ (Strem chemicals, 99,9%) at 0.1 M at pH = 6.5, 4, 2, and 1 (adjusted by HCl) was introduced in turn into the cell and again, the evolution of the spectra was followed each 20 minutes until no evolution was observed.

In situ hard XRR measurements were performed at 27 keV (λ=0.4592 Å) on the BM32 beamline at the European Synchrotron Radiation Facility (Grenoble, France) using a special cell dedicated to analysis in aqueous solution. Hard X-rays are required to cross the aqueous solution. However, to avoid damage to

the grafted molecules during the analysis, two Cu absorbers were used to decrease the beam photon flux. The evolution of the sample surfaces was observed first in ultrapure water and second, in 0.1 M $Nd(NO_3)_3$ at pH = 1 adjusted with HNO_3. Here too, the reflectivity was collected until no evolution was observed. The data obtained were rescaled from the illuminated surface area, normalized to the direct beam I0 and then plotted in the standard $I/I0.q^4$ vs. q The electron density profiles were also obtained by fitting the experimental data with the Firefx4c_6 software.

RESULTS AND DISCUSSION

Grafting process

The contact angle and also, the density and the thickness of the DGA layer extracted from the electron density profiles obtained from the XRR analyses (Figure S3 (a) and (b) in supporting information) for a grafting duration of 30 min, 1 h and 19 h are depicted in Figure 1 (a) and (b) respectively. The water contact angle increases from 10° for the activated Si wafer to a value comprised between 62° and 63° from 1h of grafting process (Figure 1 (a)). This value close to the one obtained in [54,55], attests to a more hydrophobic sample surface after the grafting. In the same way, the thickness of the DGA layer remains between 15 and 21 Å from 30 min of grafting process (Figure 1 (b)). However, the layer thickness is below the calculated length of the grafted DGA (15 Å at 1h and 21 Å at 19h vs. 26 Å), meaning that grafted molecules are not perfectly vertically oriented. Polycondensation and/or interactions between the head groups of adjacent molecules, which can tilt the molecules if there are some gaps or defects [56] in the layer, may be the cause of this difference. This may also explain the DGA layer electron density lower than the estimated electron density of bulk DGA (Figure 1 (b)). In addition, it is noteworthy that after 19h of grafting process the layer density exceeds the estimated density of bulk DGA. The presence of copper within the layer used as catalyst during the DGA synthesis may explained this result.

From the electron density profiles, the molecule surface densities were calculated for 30 min and 1h of grafting process and are of 0.5 and 1.1 grafted $DGA.nm^{-2}$ respectively. Taking into account an activated

silica surface having a hydroxyl group surface density of 5.9 Si-OH.nm^{-2} [57], it means that 2 to 6 DGA can condense on one nm^2 of the activated silica surface. The calculated molecule surface densities lower than 2 DGA.nm^{-2} indicate that some ethoxy groups remain unhydrolyzed and/or that polycondensed molecules are present.

In order to better understand the local structure of the grafted DGA, the grafting process was studied by *in situ* FTIR-ATR. Figure 2 presents the evolution of the infrared spectra of the surface of the activated Ge crystal (crystal used for the FTIR analysis in ATR mode and used as substrate) during its grafting in toluene as a function of time. The focus is set on two specific regions: (i) the stretching vibration of C=O bond ($\nu_{C=O}$) for 2° amides at a wavenumber of 1648 cm^{-1}, which is additionally characteristic of the amount of grafted DGA in the probed volume (blue arrow in Figure 2) and (ii) the peaks in 1000 –1200 cm^{-1} region corresponding to the stretching vibration of Si-O-Si (ν_{SiOSi}) bond and Si-OCH$_2$CH$_3$ ($\nu_{Si-OC\ _2CH_3}$) characteristic of the structure and arrangement of the grafted DGA molecules [58,59] (red arrow in Figure 2).

To determine the evolution of the amount of probed grafted DGA, the region around 1650 cm^{-1} presenting two peaks corresponding to the 2° and 3° amides [58,60] (amides after the triazole group and at the end of the DGA group respectively) was decomposed in two contributions: (i) a peak corresponding to $\nu_{C=O}$ of 2° amides at 1648 cm^{-1} and (ii) a peak of $\nu_{C=O}$ of 3° amides at 1675 cm^{-1}. Only the evolution of the area of the $\nu_{C=O}$ band at 1648 cm^{-1} (2° amides) was plotted as a function of time and is depicted in Figure 3 (b). The area increases until 4 h and then reaches a plateau representing the end of the grafting. This result goes with the ones obtained previously using water contact angle measurements and X-ray reflectivity. To confirm the evolution of the grafted DGA at the activated Ge crystal surface, the fraction of probed toluene was calculated subtracting a weighted spectrum of toluene from the ones of the grafting kinetics until the intensity of the characteristic toluene peaks at 1803 cm^{-1} and 1734 cm^{-1} of the aromatic combination bands [61] was zero. The evolution of the obtained fraction of probed toluene presented in Figure 3 (b) shows a decrease until 3 h and a plateau for a longer duration.

The structural evolution of the probed grafted DGA was followed studying the evolution of the peaks comprises between 1000 and 1200 cm^{-1} as displayed in Figure 2 and highlighted by a red arrow. These stretching vibrations are characteristic of $v_{Si-OC\ \ {}_2CH_3}$ and v_{SiOSi} in a cage-like or ladder-like structure [59] and thus, characteristics of the structure of the grafted DGA molecules [58,62,63]. An example of infrared spectrum of the grafted Ge surface in the 900-1200 cm^{-1} region with the various peaks identified is presented in Figure 3 (a). The peak at 1080 cm^{-1} (dark blue Figure 3 (a)) includes also the low absorption of the carbonyl groups which was neglected here.

From the areas of the various peaks present in this region, three ratios Ri characteristic of the grafted DGA structuration were calculated:

(i) the ratio R1 (1) characteristic of the structure of polycondensed DGA molecules present at the surface,

$$R1 = \frac{A_{1130cm^{-1}}}{A_{1023cm^{-1}}} \qquad (1)$$

with $A_{1130cm^{-1}}$the area of the peak corresponding to cage-like structure and $A_{1023cm^{-1}}$ the area of the peak for a ladder-like structure [58].

(ii) the ratio R2 (2) related to the polycondensation of DGA molecules,

$$R2 = \frac{A_{1023cm^{-1}} + A_{1130cm^{-1}}}{A_{1648cm^{-1}}} \qquad (2)$$

with $A_{1648cm^{-1}}$ the area of the peak corresponding to $v_{C=O}$ of 2° amides.

(iii) the ratio R3 (3) that corresponds to the presence of uncondensed groups of grafted DGA molecules,

$$R3 = \frac{A_{1158cm^{-1}}}{A_{1648cm^{-1}}} \qquad (3)$$

with $A_{1158cm^{-1}}$ the area of the peak at 1158 cm^{-1} specific for ethoxy groups bound to Si atoms [64].

The evolutions of R1, R2, and R3 presented in Figure 3 (b) highlights several phenomena. First, the grafted DGA molecules are partially uncondensed and polycondensed (R2 and R3 > 0) and have mainly a cage-like arrangement as attested by the value of R1 > 1 [58]. The formation of these structures may lead to a 3 dimensional nanoporous grafted layer. These results are consistent with the molecule surface

density calculated from X-ray reflectivity data lower than 2 grafted DGA.nm^{-2} indicating that some of the Si-OCH_2CH_3 groups are not grafted to the surface. Second, all the ratios present a decrease as a function of time until a plateau is reached after 1 hour. Therefore, this plateau is reached before the end of the complete grafting process at 4 hours highlighting a grafting process occurring in two stages.

During the first stage, before 1 hour, the degree of polycondensation of the DGA molecules grafted decreases as well as the fraction of uncondensed groups (R1 and R2 decreasing). At this end of this stage, more than 80 % of the DGA are grafted (Figure 3 (b)). During the second stage, between 1 hour and 4 hours, the remaining 20% of fresh DGA grafted do not modified the structure of the layer as attested by the constant values of R1, R2 and R3.

In order to better understand the structuration of the DGA layer, the sample grafted during 1 hour was analyzed using peak force measurements using AFM as in the literature [44]. The AFM images are presented in Figure S4 (a) and (b) and the recorded forces exerted over the tip as a function of the tip position for the activated Si substrate and for the activated Si substrate grafted with DGA during 1 hour are shown in Figure 4 (a). The results obtained from the 5 curves performed on the DGA grafted Si surface at various location at the sample surface are close to the ones obtained with activated Si substrate demonstrating the homogeneity of DGA layer on the sample surface. However, one strong vertical jump on the retract curve can be observed for the activated Si substrate at Z = -7.14 nm and an adhesion force of F = −2.19 nN and two jumps for the DGA grafted Si surface between Z= - 7.62 nm and F = - 2.51 nN; Z= -7.48 nm and F= -1.25 nN. The presence of two rupture events is probably due to the presence of two different types of grafted DGA molecules that differ by their orientations on the surface or by their degree of polycondensation [44] as illustrated on Figure 4 (b). These results are supported by the distributions of events occurring before the rupture as a function of their elongation and energy presented in Figure 4 (c) and (d), respectively. For activated Si substrate more than 90% of rupture events occur at an elongation around 0.8 nm for energy around 7 kT while for DGA grafted sample, 40 % of events occur at an elongation of 0.7 nm and 27 % at an elongation of 1 nm for energy around 10 kT. This shows that whatever

the sample, most of rupture events occur at low energy and that the tip has stronger interaction with the DGA grafted sample than the activated Si substrate.

All of these results show the formation of a layer having a homogenous surface with probably the presence of 2 types of molecules having a different degree of polycondensation and/or orientation. These data are consistent with the results obtained from X-ray reflectivity analysis and *in situ* ATR-FTIR.

According to these results from *ex situ* and *in situ* characterizations, the grafting process can be illustrated as proposed in Figure 5. During the first hour of the grafting process, polycondensed species are grafted onto the surface. Between 1h and 4h hours of the grafting process, the residual Si-OH bonds on the surface still condense with DGA molecules having a low degree of polycondensation until a complete coverage of the surface.

Interaction of Nd solution with DGA grafted molecules

To determine the grafted DGA molecule behavior in contact with a solution containing Nd^{3+} cations, the DGA layer formed at the activated Ge crystal surface previously analyzed in toluene (21 h of grafting) by in situ ATR-FTIR was analyzed in water and in aqueous 0.1 M $NdCl_3$ solution at pH = 6.5, 4, 2 and 1. In this pH range, the N-H group presents in the DGA function is neutral and thus the sample surface is neutral (Figure S5). The evolution of in situ ATR-FTIR spectra of the DGA layer in these $NdCl_3$ solutions at the equilibrium (few hours) as a function of the pH is presented on Figure 6 (a) to (c).

When the DGA layer is in contact with $NdCl_3$ solution at pH > 1, the intensity of the O-H stretching (ν_{O-H}) and H_2O bending bands (δ_{H2O}) is higher than the same bands obtained in pure water. Several phenomena may explain these results. First, highly hydrated Nd^{3+} ions diffuse inside the layer. Due to their mean hydration shell of around 9.0 H_2O molecules [65] and to their kosmotropic properties, Nd ions bring more water inside the organosilane layer that leads to an increase of the peak intensities. In addition, the intensity of ν_{O-H} and δ_{H2O} bands decrease with the pH from pH = 4 to pH 1. This tendency goes with the order of extraction efficiency of a very similar DGA functional group in the work of Winkler et al. [21]: pH = 4 < pH = 2 < pH = 1. When the pH decreases, the complexation of Nd^{3+} increases leading to

a gradual Nd^{3+} desolvation. Indeed, to be complexed, 1 to 3 DGA functions are required [66]. This desolvation explains the decrease of ν_{O-H} and δ_{H2O} bands intensities. Moreover, the intensity of ν_{O-H} and δ_{H2O} bands at pH = 4 are higher than the one at pH = 6.5 This may be explained by the contribution of Cl^- having a hydration shell of 6 H_2O molecules which may also diffuse inside the DGA layer to compensate Nd^{3+} and/or to adsorb on Ge-OH_2^+. All of these tendencies are consistent with a change of molecule arrangement at pH = 1. Indeed, the spectra in the 1360 -1330 cm^{-1} and 1420 – 1360 cm^{-1} regions characteristic for the stretching vibrations of C-N (ν_{C-N}) and the bending vibrations of alkyl bonds Si-R (δ_{asC-H}) at 1398 cm^{-1}, CH_2 (δ_{sC-H}) at 1385 cm^{-1} and, CH_3 (δ_{sC-H}) at 1370 cm^{-1} are modified at pH = 1 (Figure 6 (b) and (c)).

In order to determine the evolution of the morphology of the DGA layer in presence of Nd solution, an activated silicon wafer grafted with DGA molecules during 1 hour was analyzed in water and in aqueous 0.1M $Nd(NO_3)_3$ solution at pH = 1 using *in situ* hard X-ray reflectivity. In a first approach, we have to notice that $Nd(NO_3)_3$ solution can be compared to $NdCl_3$ solution since no ion pair is formed in both solutions as attested by small and wide-angle X-ray scattering analysis presented in Figure S6. The experimental and simulated X-ray reflectivity data and the electron density profiles associated at the equilibrium, 4h in water and 6h in $Nd(NO_3)_3$ solution, are presented in Figure 7 (a) and (b).

The electron density profile of the DGA layer obtained in water highlights the diffusion of water molecules mainly in the hydrophilic part of the DGA layer, *i.e.* in the diglycolamide headgroup zone. From the area under the curve of the difference between the electron density profiles of the sample in water and the one obtained at the laboratory atmosphere (Figure 7 (c)), 14.6 H_2O/DGA is obtained.

In $Nd(NO_3)_3$ solution at pH 1, the solution diffuses in the totality of the DGA layer. The complexation of Nd^{3+} changing the DGA conformation as observed previously by FTIR-ATR may explain this phenomenon. Here, taking into account that Nd^{3+} can be complexed by 1 to 3 DGA, $(Nd(DGA)_n^{3+}$ with n=1, 2 or 3)[58], the surface density of complexed Nd^{3+} is comprised between 0.4 (n=3) and 1.1 (n=1) $Nd^{3+}.nm^{-2}$. From these values and considering that the remaining electrons within the DGA layer (Figure

7 (c)) correspond to $Nd(H_2O)_9^{3+}$, between 1.3 (n=1) and 1.5 (n=3) $Nd(H_2O)_9^{3+}.nm^{-2}$ can be deduced. This corresponds to 9.8 to 10.9 H_2O/DGA. Even if these calculations neglect the NO_3^- contribution and maximized the amount of $Nd(H_2O)_9^{3+}$ within the DGA layer, the value obtained are in good agreement with FTIR results. Indeed, the H_2O/DGA ratio in $Nd(NO_3)_3$ solution is lower than that obtained in pure water as indicated by the intensity of the ν_{O-H} and δ_{H2O} bands (Figure 6 (a)). More details about the calculations are presented in supplementary information.

The behaviors of the grafted DGA and Nd^{3+} during interaction with each other in aqueous solution are summarized in Figure 8.

CONCLUSIONS

In this study, well-characterized model system made of functionalized organosilanes grafted on planar substrate were *in situ* characterized by FTIR-ATR and hard X-ray reflectivity in aqueous Nd solution. Using this method, for the first time, we determined experimentally that the complexation of Nd^{3+} by DGA goes with its desolvation and a modification of the DGA configuration that depend on pH.

Currently, the studies about the interactions between REE and DGA functions anchored at material surface come from extraction studies, quantifying the REE concentration in solution, or from *ex situ* spectroscopic characterizations of the hybrid material after extraction (nuclear magnetic resonance, infrared and X-ray photoelectron spectroscopies) [14-25] but not from *in situ* characterization.

With this method, other organosilane molecules having various configurations, chain lengths, headgroups *etc* can be tested in different aqueous solutions at various pH, temperature and ionic strength. In addition, this method associated to *in situ* long-period X-ray standing waves coupled to fluorescence detection for these model systems immersed in aqueous solution with a mixture of lanthanides may help to determine as in [25] the center of REEs adsorption and to precise the selectivity [67] of the organosilane molecules. Finally, coupled to theoretical methods, these results may help to provide valuable insight on the impact of molecule configurational changes during its interaction with REEs and thus to the overall free energy of extraction.

ACKNOWLEDGMENTS

This work is based on experiments performed at the BM32 french CRG beamline of the European Synchrotron Radiation Facility in Grenoble, France. Beamtime allocation for the project is gratefully acknowledged. The authors would like to thank Alban Jonchere for the support during the FTIR-ATR measurements, Guilhem Quintard and Sandra Maynadié for the maintenance of the X-Ray reflectivity and NMR tools.

Author Contributions

Oliver Walker: Investigation, Writing - Original Draft **Diane Rébiscoul**: conceptualization, Investigation Writing - Original Draft, Methodology, Supervision **Michael Odorico**: Investigation **Samuel Tardif**: Investigation **Stephane Pellet-Rostaing**: Funding acquisition **Guilhem Arrachart**: Resources, Investigation, Supervision, Writing - Review & Editing

REFERENCES

1. European Commission, Study on the Review of the List of Critical Raw Materials: Executive Summary. **2017**.
2. Bobba, S.; Carrara, S.; Huisman, J.; Mathieux, F.; Pavel, C. European Commissio, Critical materials for strategic technologies and sectors in the EU-a foresight study. *Publications Office of the European Union,* **2020**
3. Mossali, E. ; Picone, N. ; Gentilini, L. ; Rodrìguez, O. ; Pérez, J. ; Colledani, M. Lithium-ion batteries towards circular economy : A literature review of opportunities and issues of recycling treatments. *Journal of Environmental Management* **2020**, *264*, 110500.

4. Lv, W.; Wang, Z.; Cao, H.; Sun, Y.; Zhang, Y.; Sun, Z. A critical review and analysis on the recycling of spent lithium-ion batteries. *ACS Sustainable Chemistry & Engineering* **2018**, *6*, 1504-1521.

5. Yao, Y.; Zhu, M.; Zhao, Z.; Tong, B.; Fan, Y.; Hua, Z. Hydrometallurgical processes for recycling spent lithium-ion batteries: a critical review. *ACS Sustainable Chemistry & Engineering* **2018**, *6*, 13611-13627.

6. Spooren, J.; Binnemans, K.; Björkmalm, J.; Breemersch, K.; Dams, Y.; Folens, K.; González-Moya, M.; Horckmans, L.; Komnitsas, K.; Kurylak, W. Near-zero-waste processing of low-grade, complex primary ores and secondary raw materials in Europe: technology development trends. *Resources, Conservation and Recycling* **2020**, *160*, 104919.

7. P. Koukkari, I. Laukkanen, S. Liukkonen, *Fluid Phase Equilibria* **1997**, *136*, 345-362.

8. Yoon, H. S.; Kim, C. J.; Chung, K. W.; Kim, S. D.; Lee, J. Y.; Kumar, J. R. Solvent extraction, separation and recovery of dysprosium (Dy) and neodymium (Nd) from aqueous solutions: Waste recycling strategies for permanent magnet processing. *Hydrometallurgy* **2016**, *165*, 27-43.

9. Wilson, A.M; Bailey, P. J.; Tasker, P. A.; Turkington, J. R.; Grant, R. A.; Love, J. B. Solvent extraction: the coordination chemistry behind extractive metallurgy. *Chemical Society reviews* **2014**, *43*, 123-134.

10. Zemb, T.; Bauer, C.; Bauduin, P.; Belloni, L.; Déjugnat, C.; Diat, O.; Dubois, V.; Dufrêche, J. F.; Dourdain, S.; Duvail, M.; Larpent, C.; Testard, F.; Pellet-Rostaing, S. Recycling metals

by controlled transfer of ionic species between complex fluids: En route to "ienaics". *Colloid and Polymer Science* **2015**, *293*, 1-22.

11. Perez, J. P. H.; Folens, K.; Leus, K.; Vanhaecke, F.; Van Der Voort, P.; Du Laing, G. Progress in hydrometallurgical technologies to recover critical raw materials and precious metals from low-concentraded streams. *Resources, Conservation and Recycling* **2019**, *142*, 177-188.

12. Tan, Q.; Deng, C.; Li, J. Innovative applications of mechanical activation for reare erath elements recovering: process optimization and mechanism exploration. *Sci. Rep.* **2016**, *6*, 19961.

13. Tunsu, C.; Petranikova, M.; Gergorić, M.; Ekberg, C.; Retegan, T. Reclaiming rare earth elements from end-of-life products: A review of the prespectives for urban mining using hydrometallurgical unit operations. *Hydrometallurgy* **2015,** *156*, 239–258.

14. Folens, K.; Leus, K.; Nicomel, N. R.; Meledina, M.; Turner, S.; Van Tendeloo, G.; Laing, G. D.; Van Der Voort, P. Fe_3O_4@MIL-101 -A Selective and Regenerable Adsorbent for the Removal of As Species from water. *European Journal of Inorganic Chemistry* **2016**, *2016*, 4395-4401.

15. Florek, J.; Giret, S.; Juère, E.; Larivière, D.; Kleitz, F. Functionalization of mesoporous materials for lanthanide and actinide extraction. *Dalt. Trans*. **2016**, *45*, 14832– 14854.

16. Hu, Y.; Misal Castro, L. C.; Drouin, E.; Florek, J.; Kahlig, H.; Larivière, D.; Kleitz, F.; Fontaine, F.-G. Size-Selective Separation of Rare Earth Elements Using Functionalized Mesoporous Silica Materials. *ACS Appl. Mater. Interfaces* **2019**, *11*, 23681−23691.

17. Florek, J.; Larivière, D.; Kleitz, F. Nanostrucutred Organosilicas Hybrids as Highly Efficient and Regenerable Sorbents for Rare Earth Extraction. ACS Symposium Series, Vol. 1224, Nanotechnology: Delivering on the Promise Volume 2, Chapter 6, pp 107-117.

18. Hu, Y.; Drouin, E.; Larivière, D.; Kleitz, F.; Fontaine, F.-G. Highly Efficient and Selective Recovery of Rare Earth Elements Using Mesoporous Silica Functionalized by Preorganized Chelating Ligands. *ACS Appl. Mater. Interfaces* **2017**, *9*, 38584−38593.

19. Hu, Y.; Florek, J.; Larivière, D.; Fontaine, F.-G.; Kleitz, F. Recent Advances in the Separation of Rare Earth Elements Using Mesoporous Hybrid Materials. *Chem. Rec.* **2018**, *18*, 1261 – 1276.

20. Kabay, N.; Cortina, J.L.; Trochimczuk, A.; Streat, M. Solvent-impregnated resins (SIRs)-methods of preparation and their applications. *Reactive and Functional Polymers* **2010**, *70*, 484-496.

21. Winkler, R.; Pellet-Rostaing, S.; Arrachart, G. Selective Extraction of REEs Thanks to One-Pot Silica Hybrid materials. *Applied Sciences* **2020**, *10*, 7558.

22. Florek, J.; Chalifour, F.; Bilodeau, F.; Larivière, D.; Kleitz, F. Nanostrucutred Hybrid Materials for the Selective Recovery and Enrichment of Rare Earth Elements. *Adv. Funct. Mater.* **2014**, *24*, 2668-2676.

23. Florek, J.; Mushtaq, A.; Larivière, D.; Cantin, G.; Fontaine, F.-G.; Kleitz, F. Selective recovery of rare earth elements using chelating ligands grafted on mesoporous surfaces. *RSC. Adv*., **2015**, *5*, 103782.

24. Estelle, J.; Florek, J.; Larivière, D.; Kim, K.; Kleitz, F. Support effects in rare earth element separation using diglycolamide-functionalized mesoporous silica. *New J. Chem.* **2016**, *40*, 4325.

25. Florek, J.; Larivière, D.; Kählig, H.; Fiorilli, S. L.; Onida, B.; Fontaine, F.-G.; Kleitz, F. Understanding Selectivity of Mesoporous Silica-Grafted Diglycolamide-Type Ligands in the Solid-Phase Extraction of Rare Earths. *ACS Appl. Mater. Interfaces* **2020**, *12*, 57003-57016.

26. Lim, M. H.; Stein, A. Comparative Studies of Grafting and Direct Syntheses of Inorganic-Organic Hybrid Mesoporous Materials. *Chem. Mater.* **1999**, *11*, 3285-3295.

27. Yokoi, T.; Yoshitake, H.; Tatsumi, T. Synthesis of amino-functionalized MCM-41 *via* direct co-condensation and post-synthesis grafting methods using mono-, di- and tri-amino-organoalkoxysilanes. *J. Mater. Chem.,* **2004**, *14*, 951-957.

28. Ramasamy, D. L.; Repo, E.; Srivastava, V.; Sillanpää, M. Chemically immobilized and physically adsorbed PAN/acetylacetone modified mesoporous silica for the recovery or rare earth elements from the waste water-comparative and optimization study. *Water Research* **2017**, *114*, 264-276.

29. Goesmann, H.; Feldmann, C. Nanoparticle functional materials. *Angewandte Chemie International Edition* **2010**, *49*, 1362-1395.

30. Huang, S. H.; Chen, D. H. Rapid removal of heavy metal cations and anions from aqueous solutions by an amino-functionalized magnetic nano-adsorbent. *Journal of hazardous materials* **2009**, *163*, 174-179.

31. Ashour, R. M.; Abdel-Magied, A. F.; Abdel-Khalek, A. A.; Helaly, O.; Ali, M. Preparation and characterization of magnetic iron oxide nanoparticles functionalized by l-cysteine: Adsorption and desorption behavior for rare earth metal ions. *Journal of environmental chemical engineering* **2016**, *4*, 3114-3121.

32. Perreault, L. L.; Giret, S.; Gagnon, M.; Florek, J.; Larivière, D.; Kleitz, F. Functionalization of Mesoporous Carbon` Materials for Selective Separation of Lanthanides under Acidic Conditions. *ACS Appl. Mater. Interfaces* **2017**, *9*, 12003−12012.

33. Florek, J.; Mushtaq, A.; Larivière, D.; Cantin, G.; Fontaine, F.-G.; Kleitz, F. Selective Recovery of Rare Earth Elements Using Chelating Ligands Grafted on Mesoporous Surfaces *RSC Adv*. **2015**, *5* (126) 103782– 103789.

34. Florek, J.; Chalifour, F.; Bilodeau, F.; Larivière, D.; Kleitz, F. Nanostructured Hybrid Materials for the Selective Recovery and Enrichment of Rare Earth Elements *Adv. Funct. Mater.* **2014**, *24* (18) 2668– 2676.

35. Matloka, K.; Gelis, A.; Regalbuto, M.; Vandegrift, G.; Scott, M. J. Highly Efficient Binding of Trivalent F-Elements from Acidic Media with a C3-Symmetric Tripodal Ligand Containing Diglycolamide Arms *Dalton Trans*. **2005**, *23*, 3719– 3721.

36. Jańczewski, D.; Reinhoudt, D. N.; Verboom, W.; Hill, C.; Allignol, C.; Duchesne, M.-T. Tripodal Diglycolamides as Highly Efficient Extractants for F-Elements New *J.Chem*. **2008**, *32* (3) 490– 495.

37. Besnard, R.; Winkler, R.; Arrachart, G.; Cambedouzou, J.; Pellet-Rostaing, S. Ion extraction applications of bilayer-structured hybrid silicas. *Mater. Chem. Front.* **2018,** *2*, 1031–1039.

38. Winkler, R.; Pellet-Rostaing, S.; Arrachart, G. Efficient and multi-function compatible click-reaction of organosilanes. *Tetrahedron Lett.* **2020**, *61*, 152145.

39. Kim, D.; Powell, L. E.; Delmau, L. H.; Peterson, E. S.; Herchenroeder, J.; Bhave, R. R. Selective extraction of rare earth elements from permanent magnet scraps with membrane solvent extraction. *Environ. Sci. Technol.* **2015***, 49*, 9452–9459.

40. Hind, A. R.; Bhargava, S. K.; McKinnon, A. At the solid / liquid interface: FTIR / ATR – the tool of choice. *Adv. Colloid interface Sci.* **2001**, *93*, 91-114.

41. Topham, P. D.; Glidle, A.; Toolan, D. T. W.; Weir, M. P.; Skoda, M. W. A.; Barker, R.; Howse, J. R. The Relationship between Charge Density and Polyelectrolyte brush Profile Using Simultaneous Neutron Reflectivity and in Situ Attenuated Total Internal Reflection FTIR. *Langmuir* **2013**, *29*, 6068-6076.

42. Schwörer, F.; Trapp, M.; Xu, X.; Soltwedel, O.; Dzubiella, J.; Steitz, R.; Dahint, R. Drastic Swelling of Lipid Oligobilayers by Polyelectrolytes: A Potential Molecular Model for the Internal Structure of Lubricating Films in Mammalian Joints. *Langmuir* **2018**, *34*, 1287-1299.

43. Sananes Israel, S.; Rébiscoul, D.; Odorico, M.; Flaud, V.; Ayral, A. Surface Properties of Alkoxysilane Layers Grafted in Supercritical Carbon Dioxide. Langmuir **2019**, *35*, 2792-2800.

44. Rébiscoul, D.; Perrut, V.; Renault, O.; Rieutord, F.; Olivier, S.; Haumesser, P. H. Alkoxysilane layers deposited by SC CO_2 process on silicon oxide for microelectronics applications. *J. of Supercritical Fluids* **2009**, *51*, 287-294.

45. Stefan, I. C.; Mandler, D.; Scherson, D. A. In Situ FTIR-ATR Studies of Functionalized Self-Assembled Bilayer Interactions with Metal Ions in Aqueous Solutions. *Langmuir* **2002**, *18*, 6976 – 6980.

46. Wehbie, M.; Arrachart, G.; Karamé, I.; Ghannam, L.; Pellet-Rostaing, S. Triazol Diglycolamide Cavitand for lanthanide extraction. *Sep. Purif. Technol.* **2016***, 169*, 17–24.

47. McGovern, M. E.; Kallury, K. M. R.; Thompson, M. Role of solvent on the silanization of glass with octadecyltrichlorosilane. *Langmuir*, **1994**, *10*, 3607–3614.

48. Ober, Firefx4c_6: raymond.ober@college-de-france.fr

49. Parratt, L.G. Surface studies of solids by total reflection of X-rays. *Phys. Rev.* **1954**, *95*, 359.

50. B.L. Weeks, B. L.; Vaughn, M. W.; DeYoreo, J. J. Direct imaging of meniscus formation in atomic force microscopy using environmental scanning electron microscopy. *Langmuir* **2005**, *21*, 8096−8098.

51. Heinz, W. F.; Hoh, J. H. Spatially resolved force spectroscopy of biological surfaces using the atomic force microscope. *Nano-technology* **1999**, *17*, 143−150.

52. Schartner, J.; Güldenhaupt, J.; Mei, B.; Rögner, M.; Muhler, M.; Gerwert, K.; Kötting, C. Universal method for protein immobilization on chemically functionalized germanium investigated by ATR-FTIR difference spectroscopy. *J. Am. Chem. Soc.* **2013**, *135*, 4079-4087.

53. Devouge, S.; Conti, J.;Goldsztein, A.; Gosselin, E.; Brans, A.; Voué, M.; De Coninck, J.; Homblé, F.; Goormaghtigh, E.; Marchand-Brynaert, J. Surface functionalization of

germanium ATR devices for use in FTIR-biosensors. *J. Colloid Interface Sci.* **2009**, *332*, 408–415.

54. Fu, Z.; Li, T.; He, X.; Liu, J.; Wu, Y. The recyleable cyclopalladated ferrocenylimine self-assembly catalytic film and investigation of its role in the mechanism of heterogenous catalysis. *RSC Adv.* **2014**, *4*, 26413–26420.

55. Sun, Y.; Chen, C.; Xu, H.; Lei, K.; Xu, G.; Zhao, L.; Lang, M. Surface modification of silicon wafer by grafting zwitterionic polymers to improve its antifouling property. *Appl. Surf. Sci.* **2017,** *419*, 642–649.

56. Hinckley, A. P.; Muscat, A. J. Detecting and Removing Defects in Organosilane Self-Assembled Monolayers. *Langmuir* **2020**, *36*, 2563–2573.

57. Brinker, C. J.; Scherer, G. W. Sol-gel Science: the physics and chemistry of sol-gel processing. *Sol-Gel Science*. Elsevier, **1990**

58. Winkler, R.; Pellet-Rostaing, S.; Arrachart, G. Tailored structuring of functionalized silsesquioxanes in a one-step approach. *Mater. Chem. Front.* **2021**, *5*, 23282337.

59. Al-Oweini, R.; El-Rassy, H. Synthesis and characterization by FTIR spectroscopy of silica aerogels prepared using several $Si(OR)_4$ and R"$Si(OR')_3$ precoursers. *J. Mol. Struct.* **2009**, *919*, 140–145.

60. Kubelka, J.; Keiderling, T. A. Ab Initio Calculation of Amide Carbonyl Stretch Vibrational Frequencies in Solution with Modified Basis Sets. 1. *N*-Methyl Acetamide. *J. Phys. Chem. A* **2001,** *105*, 10922–10928.

61. Mirji, S. A.; Halligudi, S. B.; Sawant, Dhanashri P.; Patil, K. R.; Gaikwad, A. B.; Pradhan, S. D. Adsorption of toluene on Si(100)/SiO_2 substrate and mesoporous SBA-15. *Colloids and Surfaces A: Physicochem. Eng. Aspects* **2006***, 272,* 220–226.

62. Bantignies, J. L.; Maurin, D.; Hermet, P.; Dieudonné, P.; Wong Chi Man, M.; Bartlett, J. R.; Bied, C.; Sauvajol, J-L.; Moreau, J. J. E. Insights into the Self-Directed Structuring of Hybrid Organic- Inorganic Silicas through Infrared Studies. *J. Phys. Chem. B* **2006**, *110*, 15797–15802.

63. Orel, B.; Ješe, R.; Vilčnik, A.; Štangar, U.L. Hydrolysis and solvolysis of methyltriethoxysilane catalyzed with HCL or trifluoroacetic acid: IR spectroscopic and surface energy studies. *J. Sol-Gel Sci. Technol.*, **2005** *34*, 251–265.

64. Tejedor-Tejedor, M.I.; Paredes, L.; Anderson, M.A. Evaluation of ATR-FTIR Spectroscopy as an "in Situ" Tool for Following the Hydrolysis and Condensation of Alkoxysilanes under Rich H_2O Conditions. *Chem. Mater.*, **1998**, *10*, 3410–3421.

65. D'Angelo, P.; Zitolo, A.; Migliorati, V.; Chillemi, G.; Duvail, M. Vitorge, P.; Abadie, S.; Spezia, R. Revised Ionic Radii of Lanthanoid(III) Ions in Aqueous Solution. *Inorg. Chem.* **2011**, *50*, 4572-4579.

66. Fryxell, G. E.; Chouyyok, W.; Rutledge, R. D. Design and synthesis of chelating diamide sorbents for the separation of lanthanides. *Inorg. Chem. Commun.* **2011** *14*, 971–974.

67. Scoppola, E.; Gochev, G. G.; Drnec, J.; Pithan, L.; Novikov, D.; Schneck, E. Investigating the Conformation of Surface-Adsorbed Proteins with Standing-Wave X-ray Fluoresence. *Biomacromolecules* **2021**, *22*, 5195-5203.

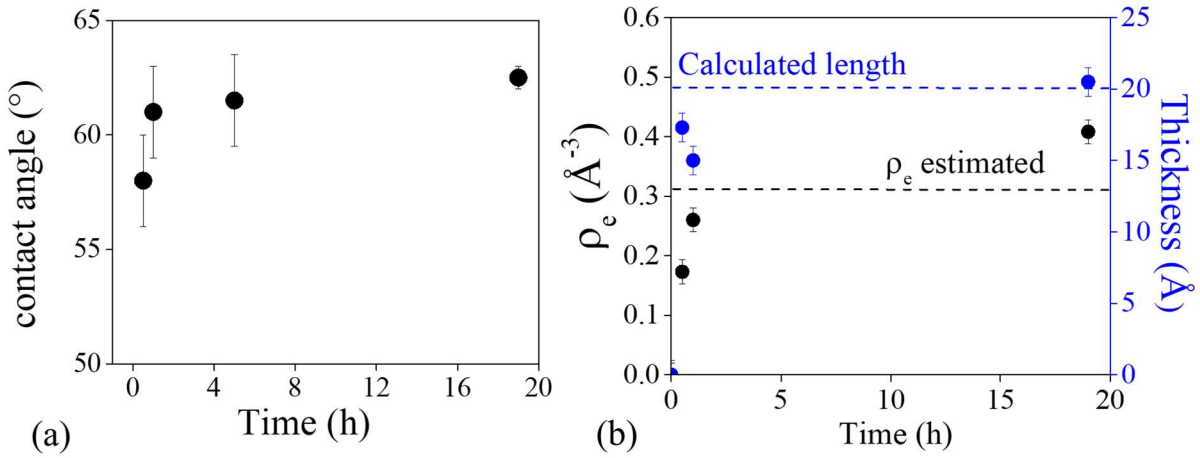

Figure 1. (a) Evolutions of the contact angle measured on the substrate after grafting and (b) of the electron density and the thickness of the grafted DGA layer obtained from the XRR simulations as a function of the grafting time. The black and blue dashed line correspond respectively to the estimated electron density calculated from mass density of the liquid organosilane and the calculated length of the grafted DGA molecule.

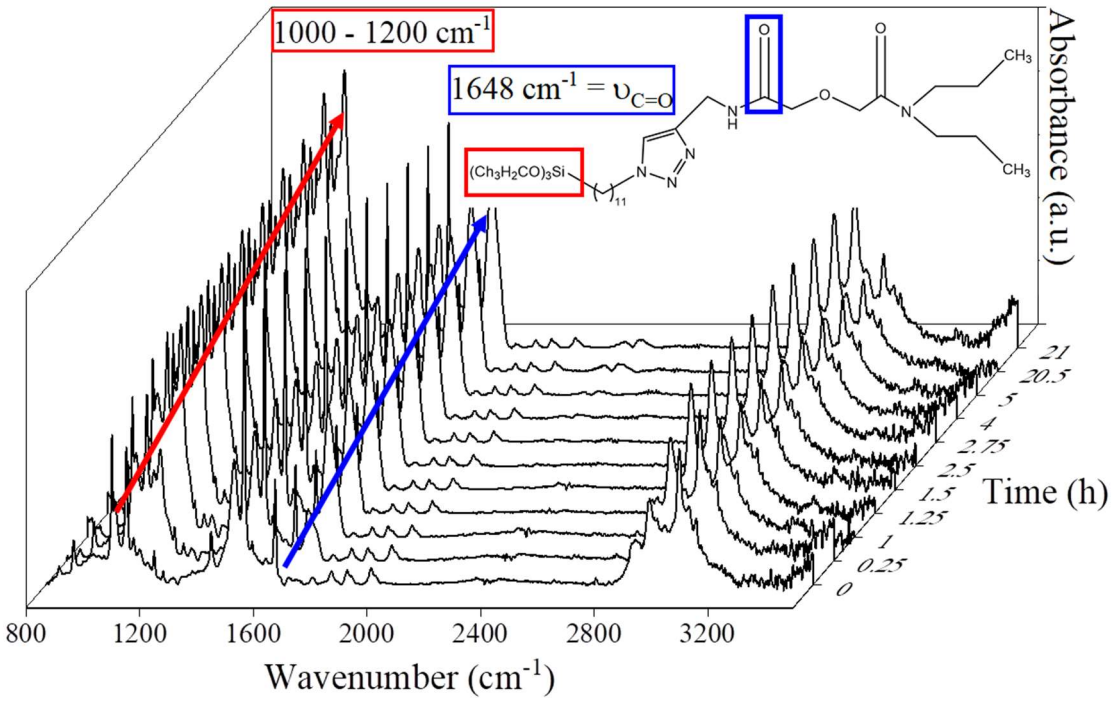

Figure 2. Evolution of the spectra of the DGA molecules grafted on the activated Ge crystal as a function of the grafting time. The blue arrow follows the evolution of $v_{C=O}$ band at 1648 cm^{-1}. The red arrow highlights the 1000 - 1200 cm^{-1} region presenting the peaks specific of v_{SiOSi} and $v_{Si-\quad {}_2CH_3}$ characteristic.

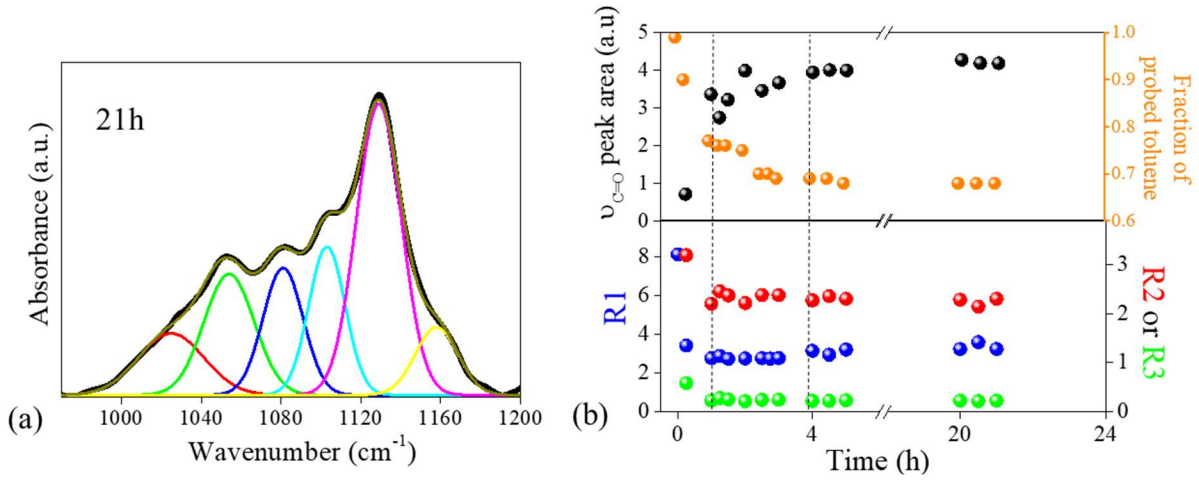

Figure 3. (a) Example of the decomposition of the infrared spectrum in 900-1200 cm^{-1} region obtained after 21h of grafting using $\upsilon_{Si-OCH_2CH_3}$ and υ_{SiOSi} peaks in a cage-like or ladder-like structure (red peak at 1023 cm^{-1}: Si-O-Si ladder-like, green and yellow peaks at 1054 cm^{-1} and 1158 cm^{-1}: Si- O-CH_2CH_3, dark blue peak: O-CH_2CH_3, clear blue and pink peaks at 1103 cm^{-1} and 1130 cm^{-1}: Si-O-Si cage-like). (b) Evolutions of the peak area corresponding to the $\upsilon_{C=O}$ at 1648 cm^{-1}, the fraction of probed toluene, the R1 (blue dot), R2 (red dot) and R3 (green dot) ratios as a function of the grafting time.

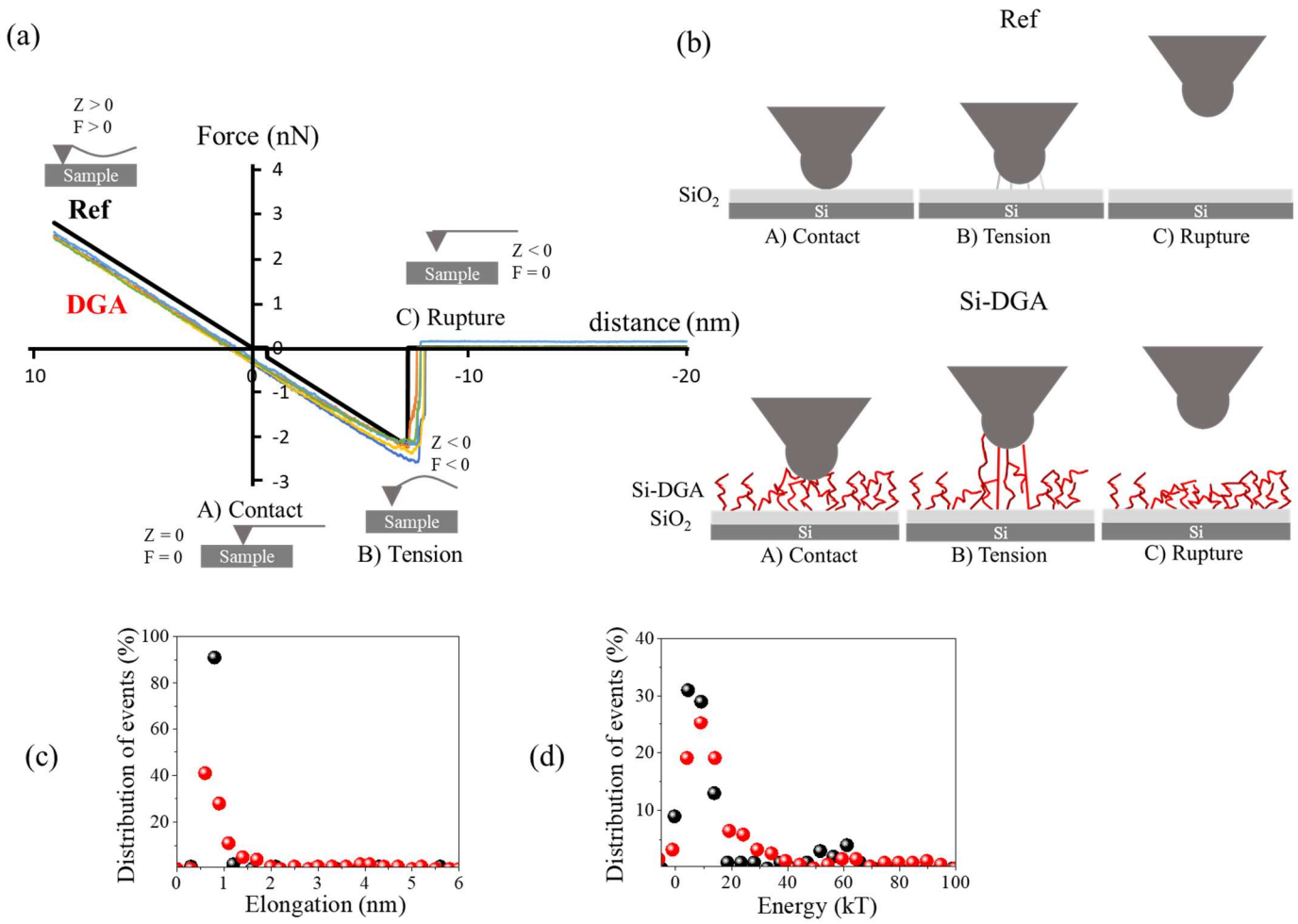

Figure 4. (a) Peak force curves recorded on activated Si substrate (Ref, black line) and on activated Si substrate grafted with DGA during 1 hour (DGA colored lines). (b) Schematic representation of the phenomena occurring during the peak force recording for the activated Si substrate (Ref) and for the DGA grafted activated Si substrate (Si-DGA). Distributions of events occurring before the rupture as a function of (c) the molecule elongation and (d) of their energy.

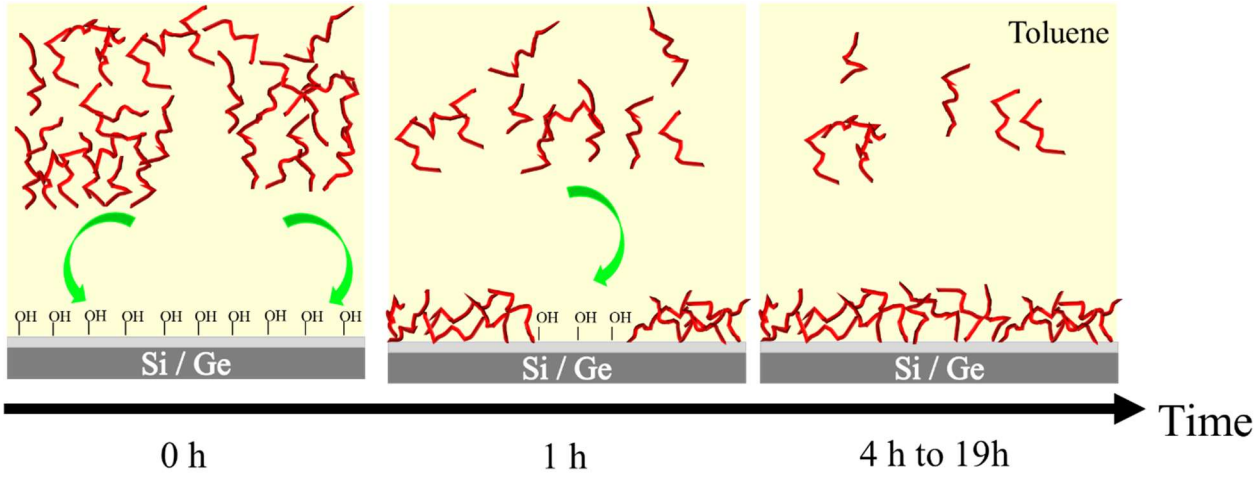

Figure 5. Proposition of grafting process of DGA molecules on activated Si or Ge substrate.

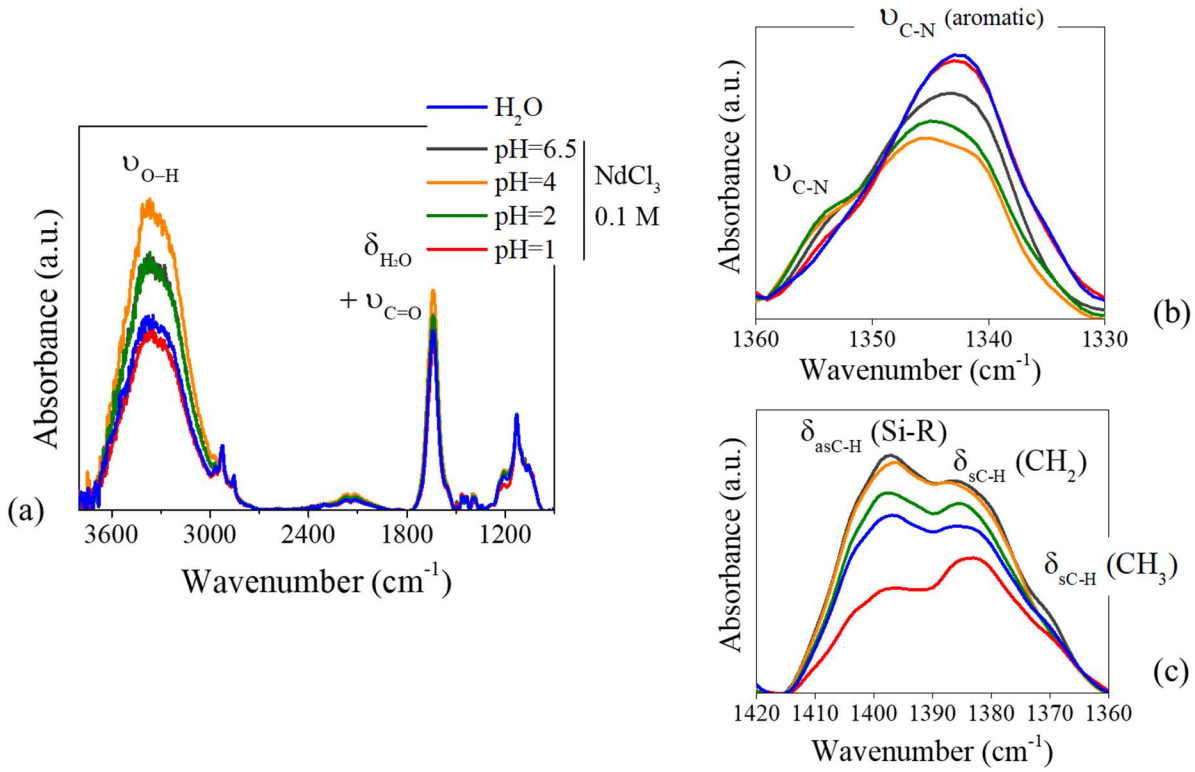

Figure 6. *In situ* ATR-FTIR spectra of the DGA molecules grafted on the activated Ge crystal in contact with water and with aqueous 0.1 M $NdCl_3$ solution at pH = 6.5, 4, 2 and 1 at equilibrium at wavelength ranges (a) 3800 – 900 cm^{-1}, (b) 1360 – 1330 cm^{-1}, (c) 1420 – 1360 cm^{-1}

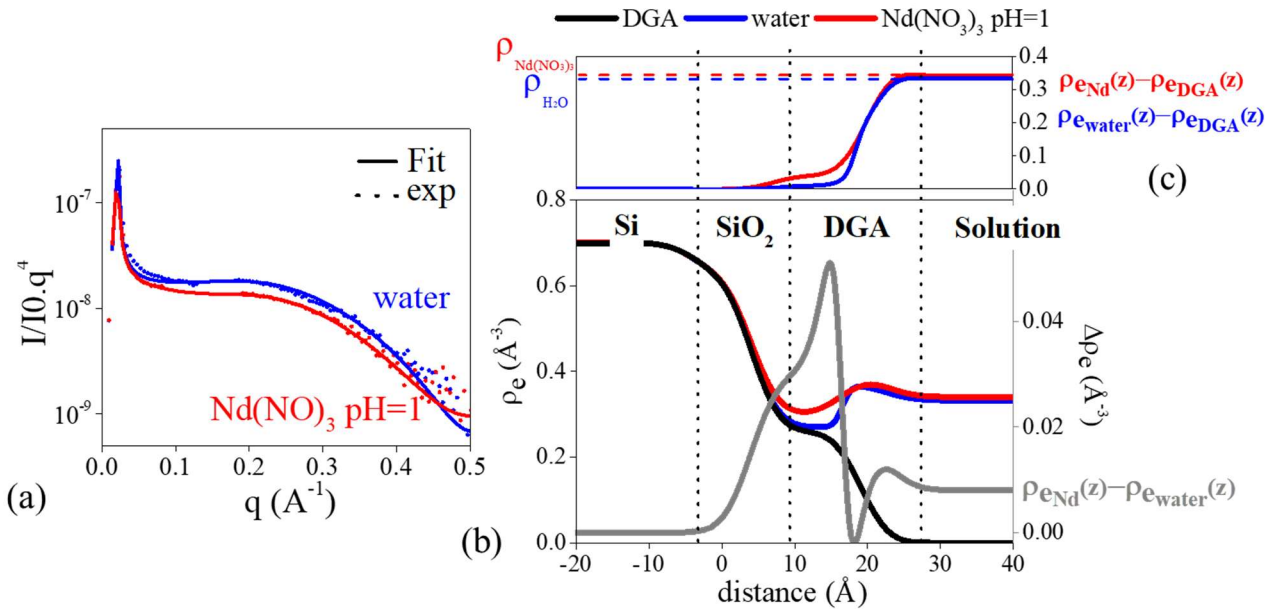

Figure 7. (a) Experimental and simulated hard X-ray reflectivity curves obtained at 27 keV and (b) associated electron density profiles of the DGA molecules grafted on the activated Si surface in water $\rho_{ewater}(z)$ and $Nd(NO_3)_3$ solution at 0.1M at pH = 1 $\rho_{eNd}(z)$ at the equilibrium (4h and 6h respectively). The electron density profile of the DGA molecules grafted on the activated Si surface $\rho_{eDGA}(z)$ measured in air at 8 keV is also presented. (c) Differences between the electron density profiles of the DGA molecules grafted on the activated Si surface in solution and the electron density profile of the DGA molecules grafted on the activated Si surface coming from measurement at 8 keV.

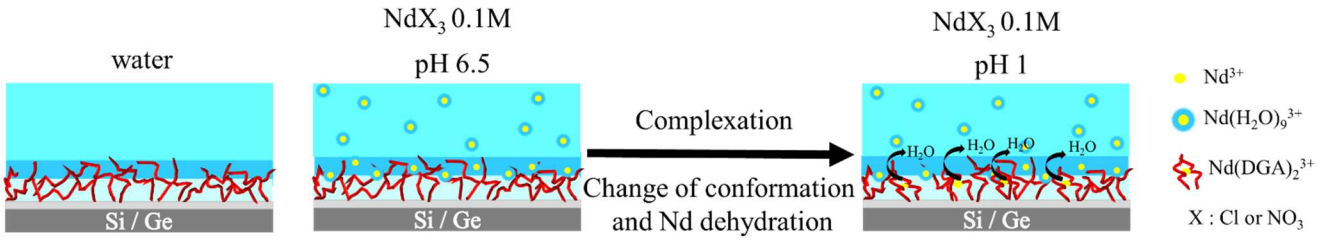

Figure 8. Illustration of the grafted DGA and Nd^{3+} behaviors in aqueous solution.

Supplementary Materials

DGA organosilane characterization

NMR

The Figure S1 presents the ^{1}H-NMR spectrum of DGA highlighting the following chemical shifts attributed to: δ = 8.01 (s, 1H, N*H*), 7.54 (s, 1H, C*H*=C), 4.56 (d, *J* = 5.8 Hz, 2H, CH_2-N), 4.27 (t, *J* = 7.3 Hz, 2H, CH_2-NH), 4.21 (s, 2H, CH_2-O-C=O), 4.08 (s, 2H, CH_2-O-C=O), 3.78 (q, *J* = 7 Hz, 6H, CH_2-O-Si), 3.34 (q, *J* = 7.15 Hz, 2H, CH_2-N), 3.17 (q, *J* = 7.15 Hz, 2H, CH_2-N), 1.85 (t, *J* = 6.82 Hz, 2H, CH_2), 1.54 (m, 4H, CH_2), 1.3-1.15 (m, 25H: 16H -(CH_2)$_8$- & 9H CH_3), 0.93 (m, 6H, CH_3-CH_2), 0.61 (t, *J* = 8.14 Hz, 2H, CH_2-Si).

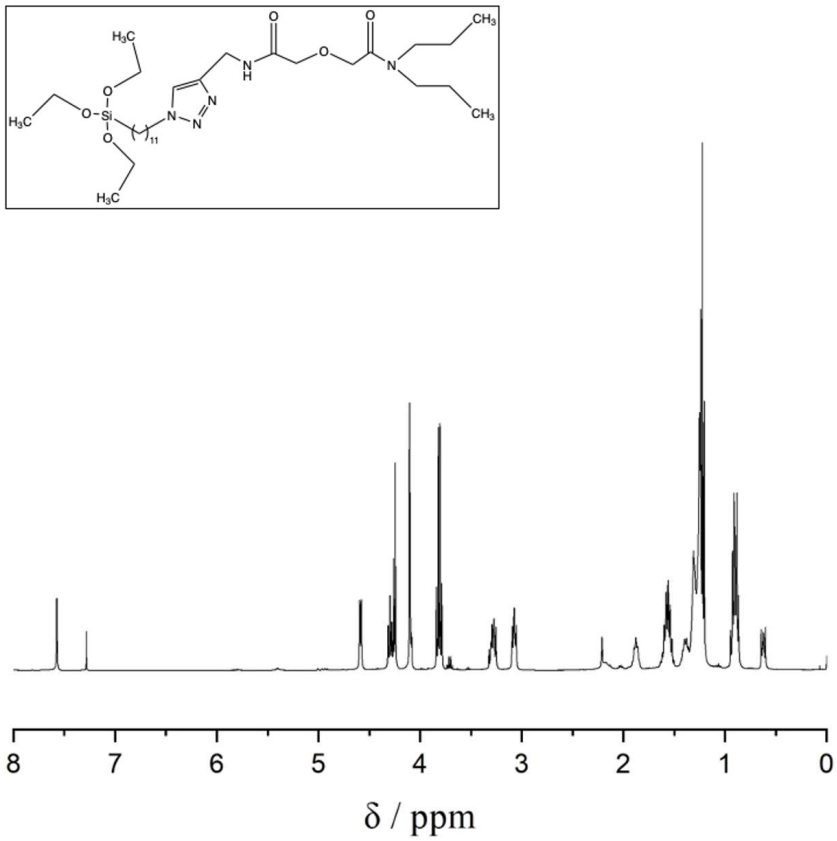

Figure S1: ^{1}H-NMR spectrum of DGA in CDCl3 at 297.9 K and 400 MHz.

FTIR

The ATR-FTIR measurements were performed by using a PerkinElmer Spectrum 100 FT-IR Spectrometer in ATR mode equipped with a DTGS/KBR detector. A drop of the fresh synthesized Si-DGA was placed on the ATR crystal and a measurement was taken while the number of scans was 4 with a resolution of 4 cm^1. The spectrum is presented in Figure S2.

The spectra display the expected peaks at 2975 cm^{-1} (ν_1) [1-2] attributed to the C-H stretching modes for CH_3 groups, at 2925 cm^{-1} (ν_2) [2] attributed to the asymmetric and at 2855 cm^{-1} (ν_3) [2] for the symmetric stretching modes for CH_2 groups, at 2095 cm^{-1} and at 1258 cm^{-1} (δ_1) attributed to the deformation mode of -CH_2 as it appears for Si-R [2]. The peak at ~ 1648 cm^{-1} ($\nu_{C=O}$), is assigned to the stretching vibration of C=O for 2° amides. For free 2° amides the peak is expected to be found at ~ 1690 cm^{-1}. [1] The red-shifted position of the peak is a typical sign for H-bonded 2° amides [3]. Furthermore, this peak is assigned to 3° amides [1] and confirming therefore the presence of the functional DGA group. The additional peak at 1460 cm^{-1} (ν_4) is attributed to the stretching modes of C=C vibrations in the triazole group supporting the success of the click-chemistry reaction [1]. As it can be seen the absorbance band at 2095 cm^{-1} ($\nu_{N=N^+=N^-}$) attributed to the asymmetric stretching mode of azido group (N_3) [4] is not present anymore confirming the conversion of the azido group in the triazole group during the click-chemistry.

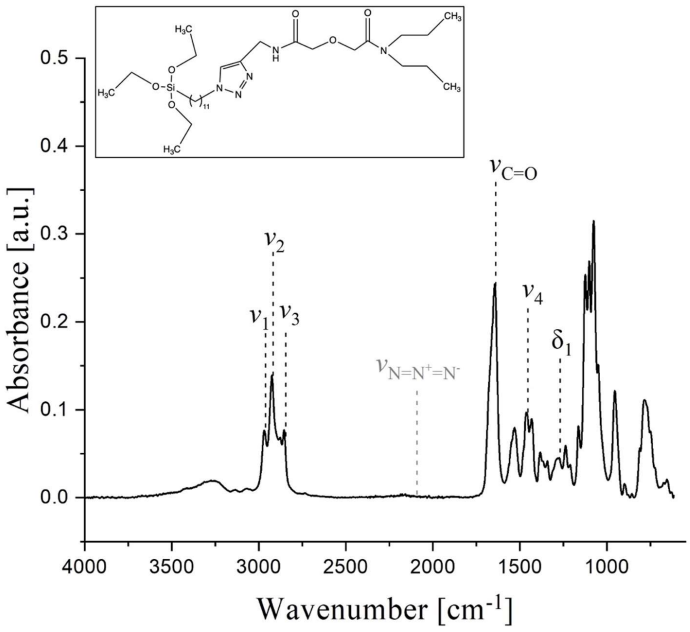

Figure S2: FTIR spectrum of DGA.

X-ray reflectivity

The Figure S3 (a) and (b) present the experimental and simulated X-ray reflectivity curves at 8 keV and the electron density profiles associated of the activated and grafted substrate as a function of the grafting duration.

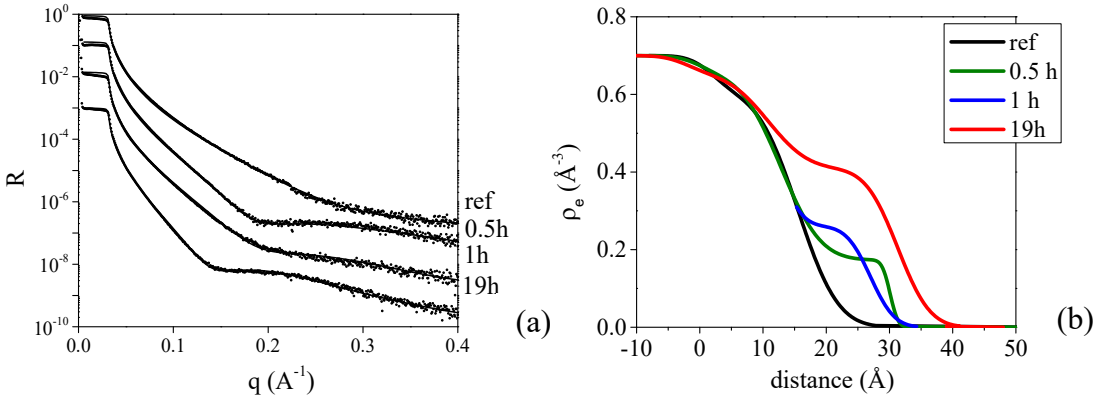

Figure S3: (a) Experimental and simulated X-ray reflectivity curves at 8 keV and (b) electron density profiles of the activated and grafted substrate as a function of the grafting duration.

AFM measurements

The recorded AFM pictures are presented in Figure S2.

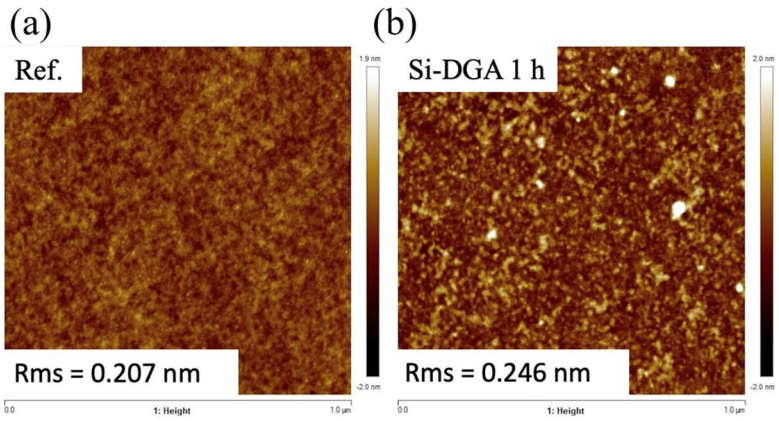

Figure S4: Picture recorded during the AFM measurements for (a) the the ungrafted Si wafer surface as a reference and (b) the surface grafted with organosilanes for a grafting duration of 1h.

Calculation of the pKa of the DGA functionalized silane using Percepta software

The Figure S5 presents the calculation results of the pKa values of the DGA functionalized silane using Percepta software. These results highlight that the molecule is not charged in the pH range of the study.

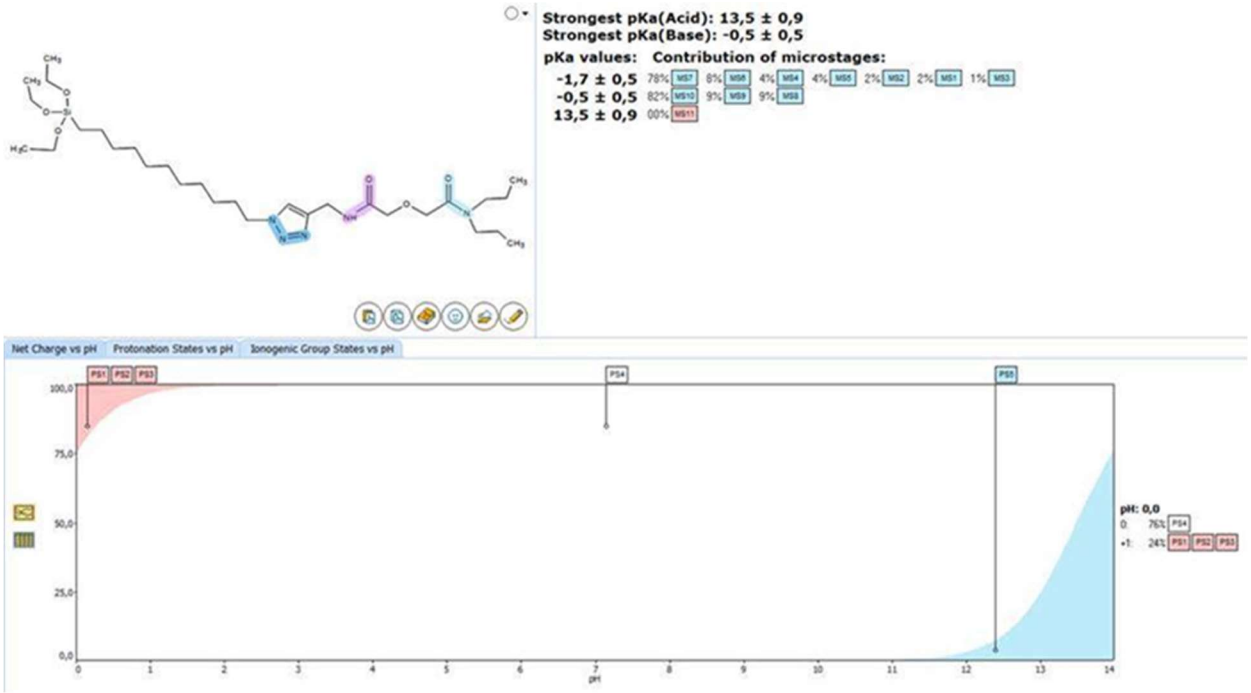

Figure S5: Small and wide-angle X-ray scattering patterns of the solutions used in the study.

Comparison of the small and wide-angle X-ray scattering patterns of the solutions.

The Figure S6 presents the small and wide angle X-ray scattering patterns of the solutions of $NdCl_3$ at 0.1 M and pH = 1, 2, 4 and $Nd(NO_3)_3$ at 0.1 M and pH 1.Whatever the solutions, no ion-pair is highlighted by these patterns.

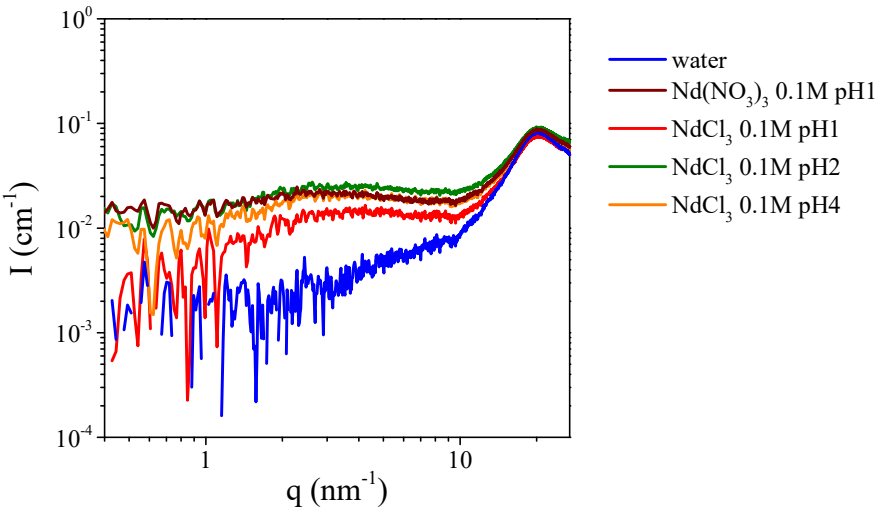

Figure S6: Small and wide-angle X-ray scattering patterns of the solutions used in the study.

Surface density calculations

The DGA, water and ion surface densities d_i (S1) were calculated from the area under the curve allowing to obtain the total number of electrons.

$$d_i = A/n_i \qquad \text{(S1)}$$

with A the area under the curve and n_i the number of electrons in the specie i considered (ions, hydrated ion and molecule). The number of electrons of the various species considered in the study are presented in the Table S1.

Table S1: Number of electrons in the various species considered for the d_i calculation.

Specie	Number of electrons
DGA	249
H_2O	18
H_3O^+	17
Nd^{3+}	57
$Nd(H_2O)_9^{3+}$	219
NO_3^-	32
$NO_3(H_2O)_6^-$	140

Water surface density when DGA layer is in water

The water surface density was calculated considering the area under the curve in the two zones, SiO_2 and DGA, described on the Figure 6 (b). The added electrons in the SiO_2 zone was considered as H_3O^+. Indeed, at the pH of ultrapure water (pH=5.7), silica surface is mainly negatively charged (PSZ=2) and H_3O^+ is adsorbed. The results are presented in Table S2.

Table S2: Water surface densities calculated at the surface of the silica and in the DGA layer and number of H_2O per DGA calculated from the DGA surface density obtained with the sample grafted during 1h.

zones	SiO_2	DGA
specie	H_3O^+	H_2O
d_i (i.nm^{-2})	0.5	16.6
H_2O/DGA (calculated with 1.1 DGA.nm^{-2})		14.6

Nd surface density when DGA layer is in $Nd(NO_3)_3$ solution at pH = 1

The electron surface density was calculated considering the area under the curve in the two zones, SiO_2 and DGA, described on the Figure 6 (b). The added electrons in the SiO_2 zone was considered as $NO_3(H_2O)_5^-$ (1 H_2O is lost when hydrated ion is adsorbed). Indeed, at pH = 1, silica surface is positively charged and the adsorption of anions is favored. The added electrons in the DGA zone were considered as Nd^{3+} complexed with DGA and $Nd(H_2O)_9^{3+}$ which has diffused within the DGA layer. Three calculations were done considering that Nd^{3+} can be complexed by 1, 2 or 3 DGA molecules. The results are presented in Table S3.

Table S3: Surface densities of species calculated at the surface of the silica and in the DGA layer and number of H_2O per DGA calculated from the DGA surface density obtained with the sample grafted during 1h.

zones	SiO_2	DGA					
$Nd(DGA)_n^{3+}$		n=1		n=2		n=3	
specie	$NO_3(H_2O)_5^-$	Nd^{3+}	$Nd(H_2O)_9^{3+}$	Nd^{3+}	$Nd(H_2O)_9^{3+}$	Nd^{3+}	$Nd(H_2O)_9^{3+}$
d_i (i.nm^{-2})	0.1	1.1	1.3	0.6	1.4	0.4	1.5
H_2O/DGA (calculated with 1.1 DGA.nm^{-2})		9.8		10.5		10.9	

References

1. Winkler, R.; Pellet-Rostaing, S.; Arrachart, G. Tailored structuring of functionalized silsesquioxanes in a one-step approach. *Mater. Chem. Front.* 2021, *5*, 23282337.
2. Al-Oweini, R.; El-Rassy, H. Synthesis and characterization by FTIR spectroscopy of silica aerogels prepared using several $Si(OR)_4$ and R"$Si(OR')_3$ precursors. *J. Mol. Struct.* 2009, *919*, 140–145.
3. Kubelka, J.; Keiderling, T. A. Ab Initio Calculation of Amide Carbonyl Stretch Vibrational Frequencies in Solution with Modified Basis Sets. 1. *N*-Methyl Acetamide. *J. Phys. Chem. A* 2001, *105*, 10922–10928.
4. Lummerstorfer, T.; Hoffmann, H. Click Chemistry on Surfaces: 1,3-Dipolar Cycloaddition Reactions of Azide-Terminated Monolayers on Silica. J. *Phys. Chem. B*, 2004, *13*, 3963–3966.